Hindawi
Journal of Nanomaterials
Volume 2021, Article ID 5576048, 11 pages
https://doi.org/10.1155/2021/5576048

Research Article

Facile Synthesis of rGO/Mn_3O_4 Composite for Efficient Photodegradation of Phenol under Visible Light

P. Shobha,[1] Albin John P. Paul Winston,[1] S. Sunil,[1] T. Manovah David,[2] S. Mary Margaret,[1] S. Muthupandi,[1] and P. Sagayaraj[1]

[1]*Department of Physics, Loyola College (Autonomous), Chennai 34, India*
[2]*Thin Films and Coatings Section, Materials Science Group, Indira Gandhi Centre for Atomic Research, Kalpakkam 603 102, India*

Correspondence should be addressed to P. Sagayaraj; sagayaraj1962@gmail.com

Received 20 January 2021; Revised 16 March 2021; Accepted 18 April 2021; Published 7 June 2021

Academic Editor: G. Ravi

To enhance reusability and to maintain higher efficiency in degradation, Mn_3O_4/rGO nanocomposites were synthesized by a facile thermal treatment. Initially, Mn_3O_4 nanoparticles were prepared and analyzed by powder XRD and HR-SEM. The composition of manganese oxide was varied to obtain different nanocomposites. The Mn_3O_4 ions were found to be well anchored onto the rGO surface. The obtained samples were taken for the photodegradation studies with phenol as the pollutant. Under a dynamic mode, the absorption efficiency was found to be maximum for the MnsR0.75 sample for phenol.

1. Introduction

Discharge of organic wastes into local water bodies has been one of the most serious issues. The highly toxic wastes in industrial effluents contain a large portion of phenolic compounds that have adverse effects on both nature and public health [1–3]. The common sources of phenolic pollution are paints, pesticides, coke ovens, coal conversion, polymeric resin, paper mills, petroleum refineries, and petrochemical and pharmaceutical industries [4–6]. These compounds have stubborn nonbiodegradable properties and toxicity and, therefore, posed to be fatally harmful to aquatic life and humans since the phenolic compounds own considerably high binding capacity in aqueous medium. Furthermore, their unpleasant odor and taste add to the detrimental effect on aqueous systems [7–10]. Thus, it is important to develop an adhesive-like material to remove the organic pollutants from water bodies to minimize pollution [11–13]. Many techniques have been used to remove phenol from wastewater such as photocatalytic degradation, membrane filtration, chemical oxidation, and solvent extraction [14–21]. Recently, Wang et al. prepared 2D/2D γ-MnO_2/rGO using rGO and $KMnO_4$ for the catalytic ozonation of 4-chlorophenol in the presence of PMS [22]. Ramesh et al. examined the catalytic efficiency of MnO_2/rGO nanowires for the degradation of reactive red using a sono-Fenton-assisted process in the presence of H_2O_2 [23]. Qu et al. used a suspension of GO/$MnSO_4$ from the modified Hummers method to fabricate rGO/MnO_2 to degrade methylene blue dye in the presence of H_2O_2 [24]. Recently, the research has turned towards the removal of pollutants via photocatalysis employing either UV or visible light [25–29]. In recent times, rGO has gained considerable attention in this area as an effective metal-free catalyst which has been used in order to weaken up the persulphate, eventually wearing away the O-O band present at the dynamic sites and forming an excellent electron bridge (Duan et al., 2015, [30]). In a similar way, nanodiamonds, cubic mesoporous carbon, and CNT have been extensively used by researchers in degrading organic pollutants [2, 31, 32]. Though these materials caused degradation of the target compounds, a longer time was required to achieve a complete degradation. Hence, graphene was employed in this work to attain a higher surface area along with unique properties such as good conductivity, charge delocalization, chemical stability, and electron transfer properties thereby making it an excellent candidate for the purpose. Graphene, with these qualities, could be considered a suitable material to be used in the degradation of organic pollutants [26, 33]. In addition,

metal oxides based on manganese have been extensively explored owing to their superior physical and chemical properties, low toxicity, and abundance. The presence of their unique redox loops leads to a higher potential activity via the single electron transfer making its way to be a suitable catalyst [34]. The additional difficulty arises due to the superfine nature of Mn as it forms a well-dispersed solution [35, 36]. In a nutshell, photocatalysis is the acceleration of photoelectrons due to the presence of a catalyst like Mn used in this case. Thus, more attention has been paid towards metal-free catalysts like carbon materials which are both cheap and environment-friendly and also for sustainable sources. In a typical heterogeneous experiment, the carbon material will be acting as an adsorbent [37], catalytic support [38], and in some cases also a catalytic support [39]. These peculiar properties make it an interesting candidate along with other properties like their stability with acids and bases, surface, texture, and mechanical and electrical properties. It is also commendable to observe that the incorporation of a carbon material induces an encouraging effect not only on the efficiency but also on the degree of degradation achieved in the reactions [40, 41]. This work is aimed at creating a metal oxide-based composite with the addition of a carbon support to facilitate a better degradation of phenol.

2. Materials and Methods

2.1. Synthesis of rGO. All the chemicals used were of analytical grade and used without any further purification. In a synthesis procedure, 1 g of graphite flakes was added to 50 ml concentrated sulfuric acid while stirring in an ice-water bath and maintaining the temperature under 10°C. 0.379 M potassium permanganate was gradually added to the above solution; the reaction was quenched by the addition of 200 ml distilled water. An extra 2 h ultrasonic treatment was carried out and processed for the preparation (reduction) of rGO. After adjusting the pH to ~6 with the addition of sodium hydroxide (0.1 M), the suspension was further sonicated for 1 h. 0.567 M of the reducing agent L-ascorbic acid was dissolved in 100 ml distilled water and then was slowly added to the exfoliated graphite oxide suspension at room temperature, to act as a mild reducing agent. The reduction was performed by maintaining the solution at 95°C for 1 h. The resultant black precipitate was simply filtered by cellulose filter paper and was further washed with a 1 M hydrochloric acid solution to wash away the remaining impurities and followed by washes in distilled water, and the pH was brought to neutral. Finally, the filtrate was freeze-dried to obtain rGO powder.

2.2. Synthesis of Mn_3O_4 Nanospheres. The sol-process is one of the easiest ways to synthesize Mn_3O_4 nanostructures. An aqueous solution consisting of manganous chloride (0.05 M) and N,N-dimethylformamide (0.01 M) was stirred on a magnetic stirrer at room temperature for 15 min. Under this stirring condition, an equal volume of 0.05 M sodium hydroxide was added drop-wise into this reaction mixture. The colorless solution turns initially to light brown and later to a dark brown colloidal precipitate, which indicates the formation of

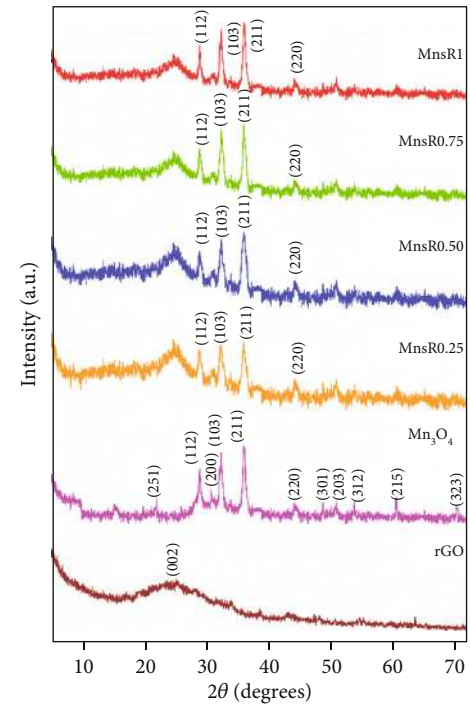

Figure 1: X-ray diffractograms of rGO, pristine Mn_3O_4, MnsR0.25, MnsR0.50, MnsR0.75, and MnsR1.

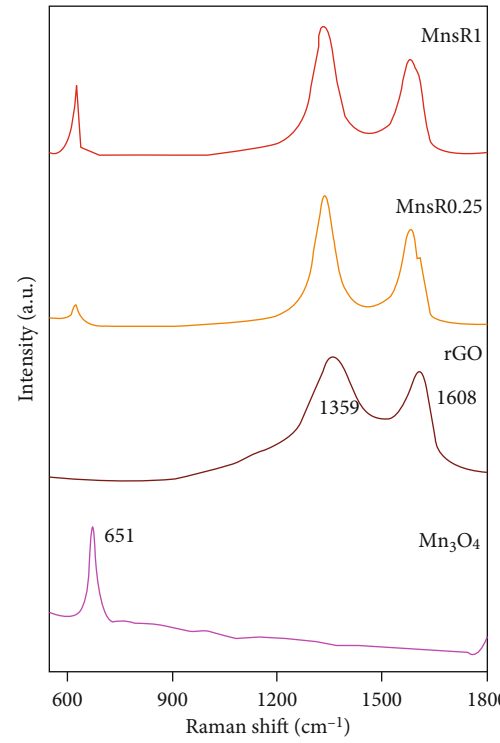

Figure 2: Raman plot of pristine Mn_3O_4, rGO, MnsR0.25, and MnsR1.

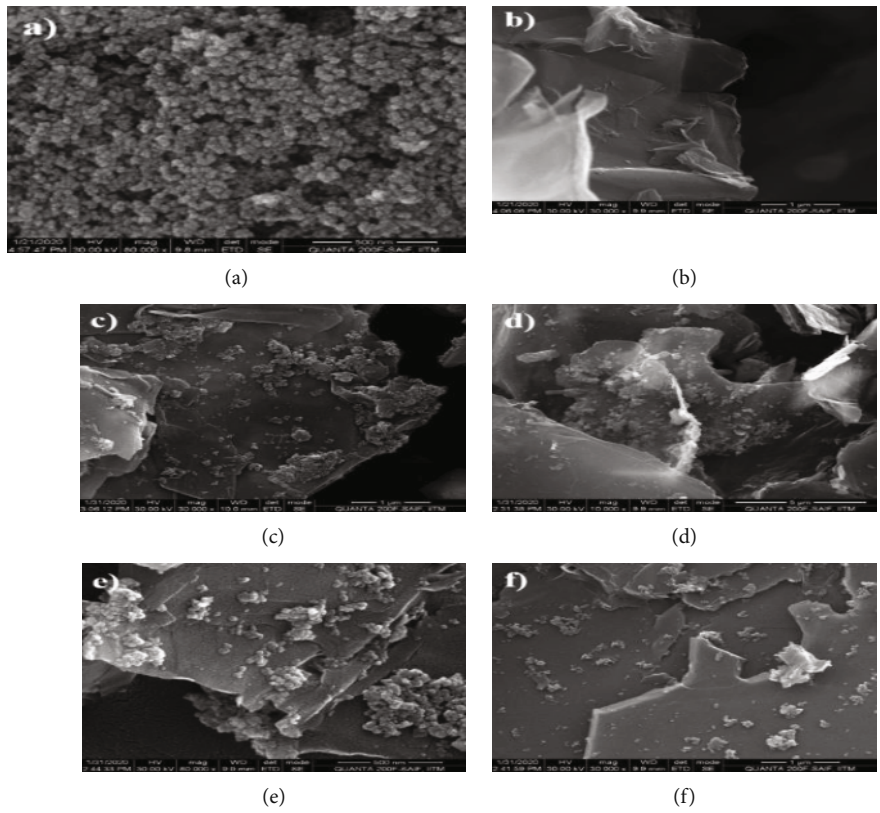

FIGURE 3: HR-SEM images of (a) pristine Mn_3O_4, (b) bare rGO, (c) MnsR1, (d) MnsR0.75, (e) MnsR0.50, and (f) MnsR0.25.

the Mn_3O_4 nanostructure. The stirring process was prolonged for 2 hours. The particles were centrifuged and washed with distilled water several times and finally with ethanol and then conventionally annealed at 400°C for 2 hours to eliminate the coordinated H_2O molecule.

2.3. Preparation of rGO/Mn_3O_4 Nanocomposites. The rGO/Mn_3O_4 nanocomposites were formed from the individually prepared rGO and Mn_3O_4 nanoparticles. Ethylene glycol aided in the composite formation process; 100 mg of Mn_3O_4 was added to 20 ml of ethylene glycol and then for an hour. A brownish-black color solution was obtained, and to this colloidal solution, an equal amount (100 mg) of rGO was added. The colloidal mixture was allowed to stir for 30 minutes and dried in an oven at 140°C to obtain the rGO/Mn_3O_4 composites. By keeping the mass of rGO a constant (100 mg), three more composites were prepared by changing the Mn_3O_4 mass as 25, 50, and 75 mg. The samples prepared with the mass of 25, 50, 75, and 100 mg are labeled as MnsR0.25, MnsR0.50, MnsR0.75, and MnsR1, respectively.

2.4. Characterization. The structural, morphological, optical, compositional, and thermal data of the as-prepared samples were investigated. X-ray diffraction was carried out on a Rich Seifert X-ray diffractometer in the range 10-75°; Raman analysis was performed with the QE Pro Raman Series Spectrometer. HR-SEM and EDX analyses were carried out on a Quanta 200 FEG High-Resolution Scanning Electron Microscope equipped with an EDAX analyzer. The FT-IR spectrum was taken on Perkin Elmer Spectrum Two within a range of 500-4000 cm^{-1}. TG thermograms were obtained from Perkin Elmer STA 6000 in the presence of nitrogen atmosphere (20 ml/hr) in the temperature range of 100-800°C.

3. Results and Discussion

Figure 1 shows the X-ray diffraction (XRD) pattern of the synthesized rGO sheets which exhibits a broad diffraction peak at 24°. The powder XRD pattern of the as-prepared Mn_3O_4 is depicted in Figure 1. These peaks were conveniently indexed to a pure tetragonal phase of the Mn_3O_4 nanostructure (JCPDS card No. 89-4837) [41]. The peaks of the composite indicate the presence of Mn_3O_4; the steady increase in the intensity of the peaks indicates the increasing presence of manganese in the composites from MnsR0.25 to MnsR1. The same has been reflected in the Raman analysis depicted in Figure 2. The XRD pattern of rGO/Mn_3O_4 nanocomposites is shown in Figure 1, and it shows no structural changes and contains perfect combinations of the above peaks corresponding to both Mn_3O_4 and rGO. The crystallite size of Mn_3O_4 nanospheres was calculated by the Debye-Scherrer formula:

$$D = \frac{k\lambda}{\beta \cos \theta}, \quad (1)$$

where D is the crystalline size, k is the shape factor, λ is the wavelength of X-ray, β is the full-width half maxima of the peak, and θ the angle at which the peak has been observed. The particle size of the Mn_3O_4 nanosphere is calculated to

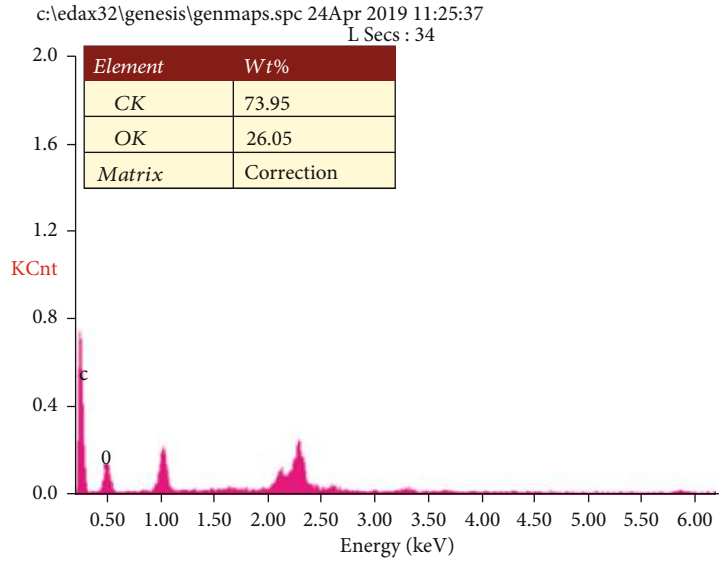

(a)

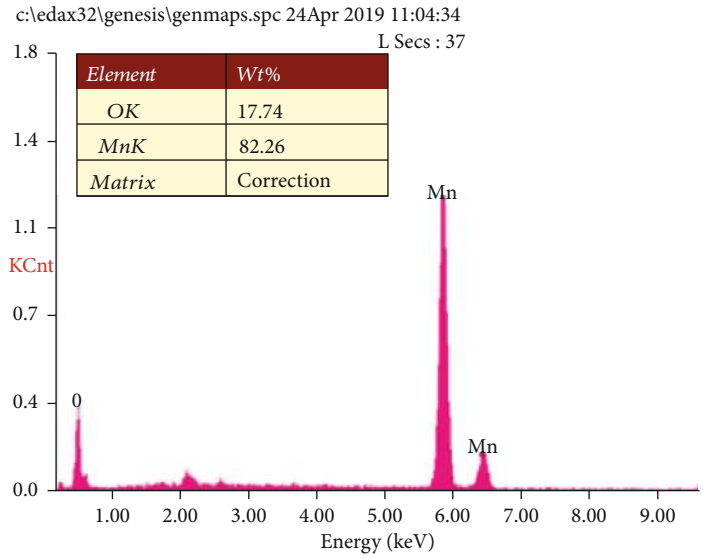

(b)

Figure 4: Continued.

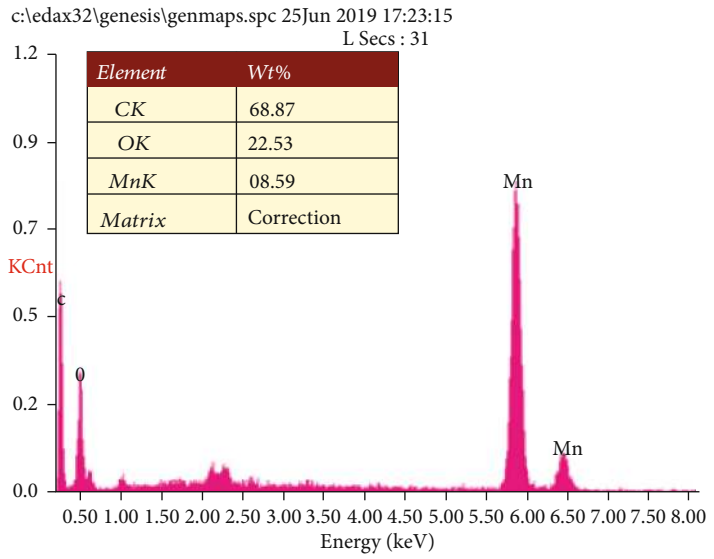

(c)

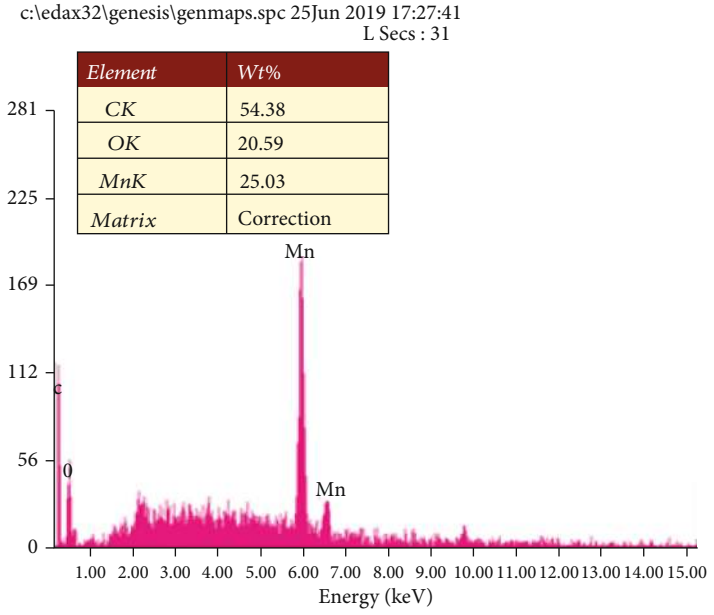

(d)

Figure 4: Continued.

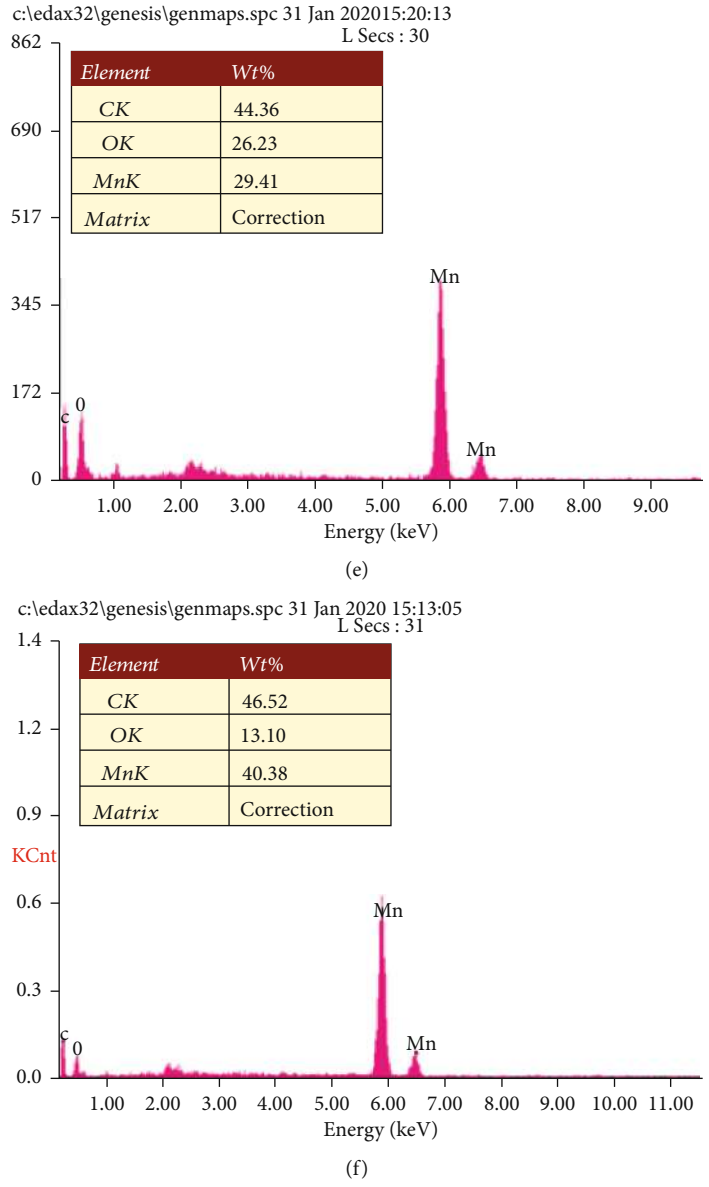

Figure 4: EDX plots of (a) bare rGO, (b) pristine Mn_3O_4, (c) MnsR1, (d) MnsR0.75, (e) MnsR0.50, and (f) MnsR0.25.

be between 15 and 25 nm. Raman spectroscopy being an important tool is used in exploring the structural properties of the materials. The sharp peak at 651 cm^{-1} depicted in Figure 2 indicates the presence of Mn_3O_4 [42]. The Raman spectra of the reduced graphene oxide is depicted in Figure 2 with the characteristic peaks at 1359 and 1608 cm^{-1} corresponding to the D and G bands of reduced graphene oxide. The G band corresponds to the radial C-C stretching of the sp^2 carbon, and the D band relates to the first-order zone boundary phonon related to the defects on the edges of graphene. The intensity ratio (I_D/I_G) of the D and G bands was used to qualitatively characterize the defect density of rGO to be 0.8451 and 0.8576 for the composite MnsR1 [43].

The obtained crystallite size is nearly the same when compared to those obtained from the HR-SEM images. Mn_3O_4 exhibits a spherical morphology while rGO demonstrated a sheet-like morphology (Figures 3(a) and 3(b)), but in an agglomerated form which is attributed to the higher adsorption of moisture from the atmosphere. Mn_3O_4 nanospheres are clearly visualized in Figure 3(a) where the nanospheres are almost in the range of 15-29 nm. Figures 3(c)–3(f) demonstrate the even coating of Mn_3O_4 onto the rGO sheets. The EDAX spectrum of the samples also describes the quantitative analysis of the as-prepared samples. Figures 4(a)–4(f) illustrate the EDAX spectrum of rGO, Mn_3O_4, and the composites. The molecular structure of the synthesized samples was studied by FT-IR spectra (Figure 5). In the range 500-4000 cm^{-1} for rGO, the broad bands observed at 3338 cm^{-1} correspond to the strong stretching mode of the OH group [44], the absorption peak at 1635 cm^{-1} corresponds to the C=C stretching mode, and the peaks at 1716, 1154, and 1033 cm^{-1} correspond to the stretching modes of C=O, C–OH, and C–O, respectively.

FT-IR spectra of the Mn_3O_4 nanoparticles with absorption peaks at 620.10 cm^{-1} and 540.09 cm^{-1} correspond to the stretching vibration of Mn–O and Mn–O–Mn bonds indicating the formation of Mn_3O_4; the peak at 1636 cm^{-1} correspond to O-H bending vibrations. Figure 5 illustrates the molecular vibrational spectra for the rGO-composed Mn_3O_4 particles. The resulting vibrations at the lower frequency region suggested the formation of the Mn_3O_4 molecular structure. The vibrations at 3462 cm^{-1} may be assigned to the O-H stretching of adsorbed water, and the absorption bands at 1112 cm^{-1} are due to the molecular vibrations of C-O. The molecular vibrational band at 1636 cm^{-1} can be related to the O-H bending and C-O stretching vibrations. Thermogravimetric analysis was conducted to understand the thermal stability of MnsR1 nanocomposites. The experiments were performed up to 800°C in a nitrogen atmosphere at a heating rate of 10°C/min. Figure 6(a) depicts the TGA of the as-prepared rGO which indicates a significant weight loss linearly until it reaches around 450°C, attributed to the higher thermal stability of the sample followed by a sudden weight loss up to 600°C. Further, Figure 6(b) illustrates the TGA of Mn_3O_4; the TG depicts clearly three different regions of weight loss. Region 1 weight loss took place from room temperature to 300°C; this weight loss has been attributed to the removal of water from the specimen, namely, physisorbed molecular water and structural water, i.e., water of crystallization and chemically bound water. Region 2 in the range 390-610°C is attributed to the reduction of Mn from the specimen, and Region 3 from 650 to 800°C is attributed to the final decomposition of the specimen. Mn has higher thermal stability in comparison to other electrocatalysts. The composite MnsR1 has a lower total mass loss (about 15 wt%) than that of rGO (Figure 6(c)). The mass loss from 200 to 400°C can be attributed to the decomposition of rGO. Since Mn_3O_4 can withstand higher temperatures (about 500°C), the composite of MnsR1 only shows a gradual mass loss when the temperature is over 500°C. The difference in the total mass loss between rGO and MnsR1 is about 15 wt%. If it is assumed that Mn_3O_4 is thermally stable and does not have a mass loss below 600°C, the amount of Mn_3O_4 loaded in the MnsR1 is about 52.0 wt%.

3.1. Photocatalytic Performance. The photocatalytic performance of the prepared samples was carried out in the presence of visible light. The stock solution was prepared by dissolving 20 mg/l of phenol in distilled water and further taken for the analysis. 50 ml of the stock solution was placed in a dark room setup in order to block the interference of any stray light. The solution was placed on a stirrer, and 30 mg of the catalyst was added and left for 30 minutes in the dark to attain the adsorption desorption isotherm; after the collection of the sample, visible light via a 20 W bulb was introduced into the dark room for 15 minutes, and again, the sample was collected. The procedure was repeated until the completion of 120 minutes. The remaining sample was withdrawn via centrifugation after every cycle in order to carry out the repetition cycles. The degradation percentage was calculated as follows:

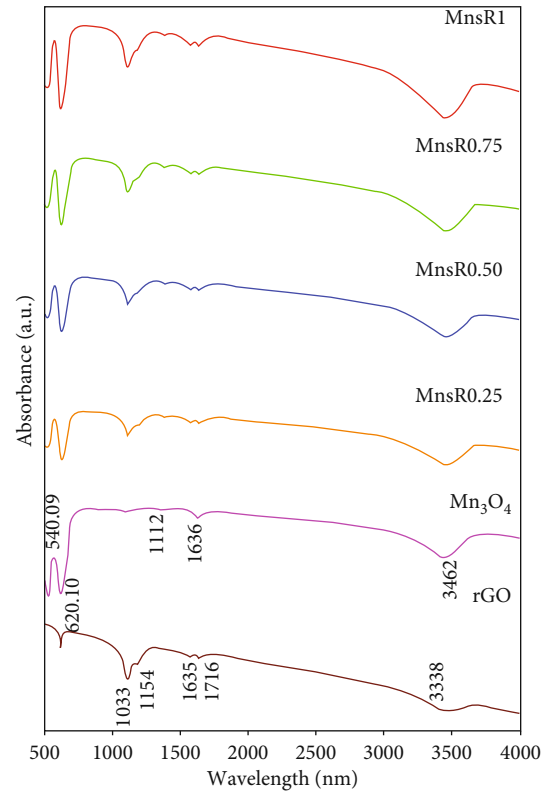

Figure 5: FT-IR spectra of bare rGO, pristine Mn_3O_4, MnsR0.25, MnsR0.50, MnsR0.75, and MnsR1.

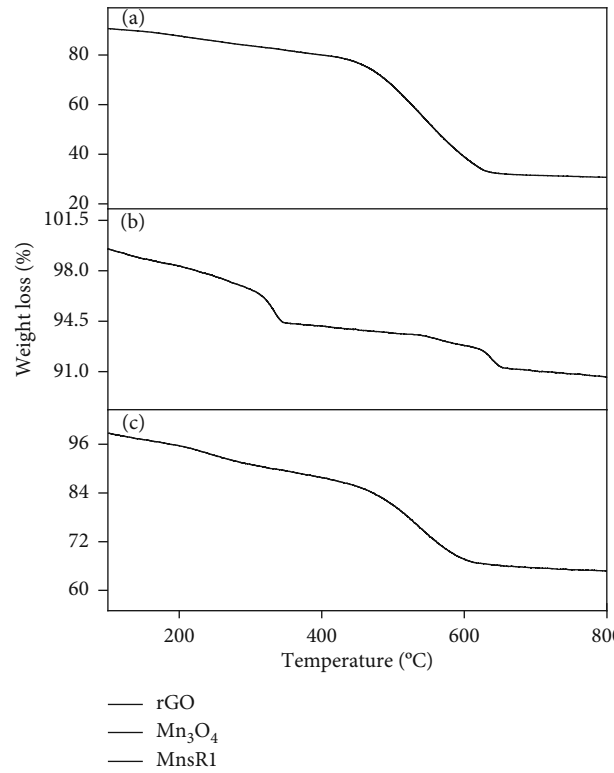

Figure 6: Thermogram of bare rGO, pristine Mn_3O_4, and MnsR1.

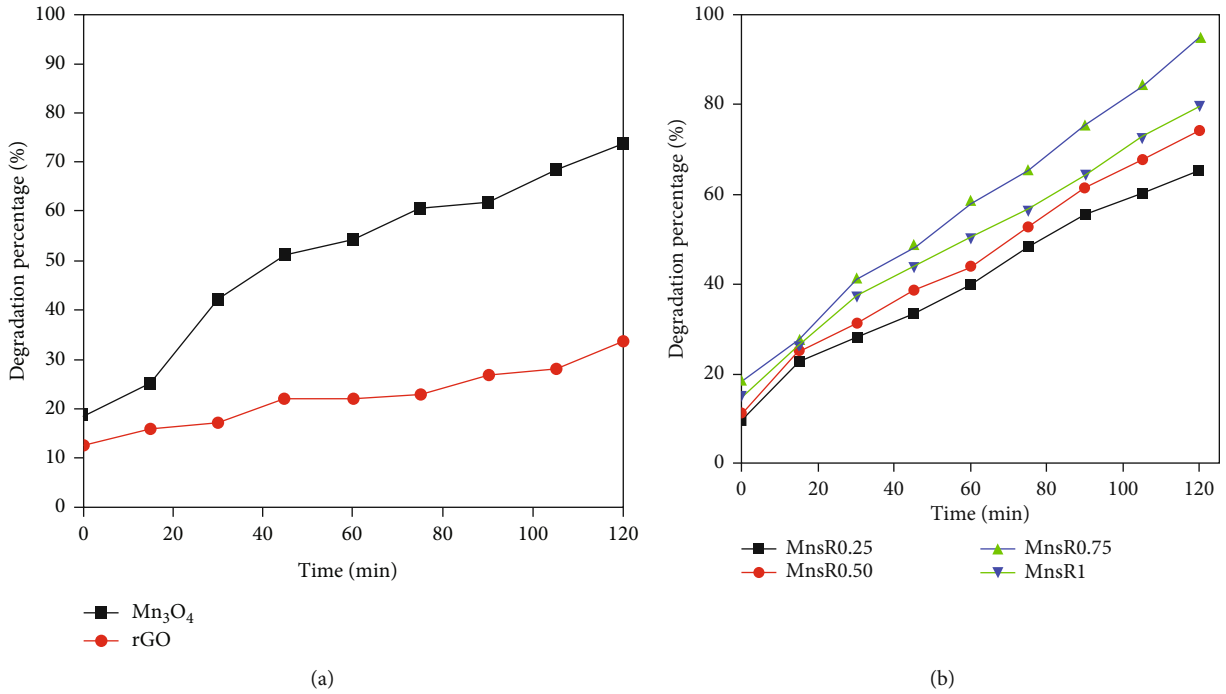

Figure 7: (a) Degradation percentage of rGO and pristine Mn_3O_4; (b) degradation percentage of MnsR0.25, MnsR0.50, MnsR0.75, and MnsR1.

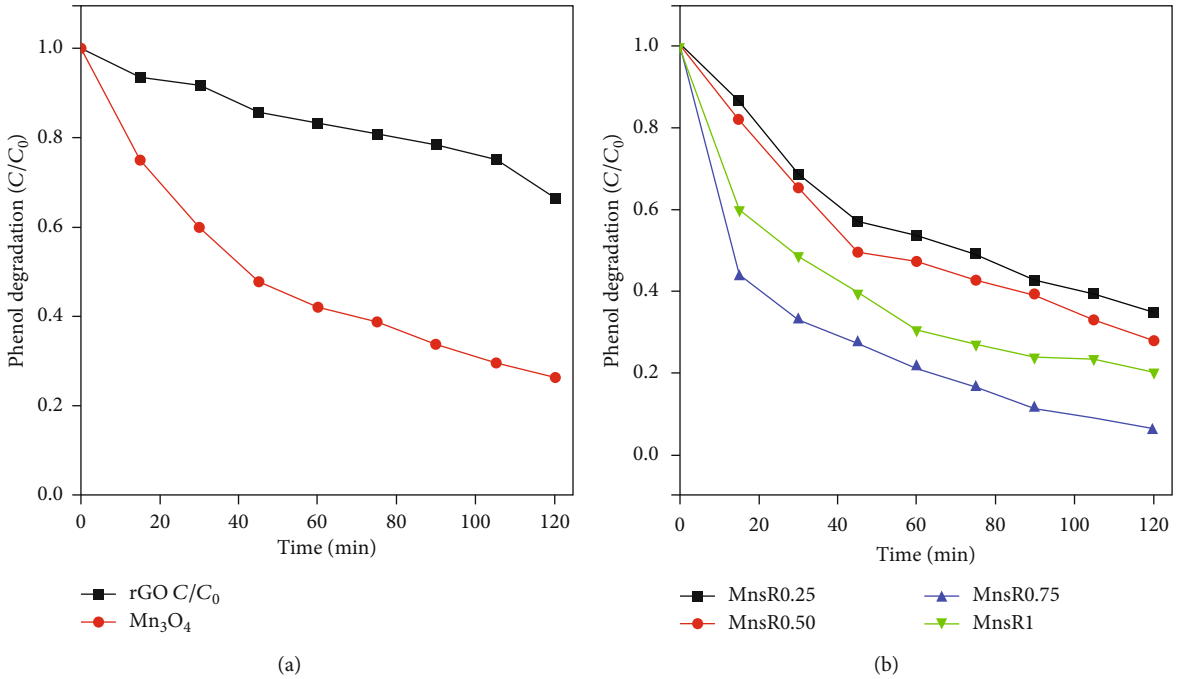

Figure 8: (a) Degradation concentration of rGO and pristine Mn_3O_4 and (b) absorbance percentage of MnsR0.25, MnsR0.50, MnsR0.75, and MnsR1.

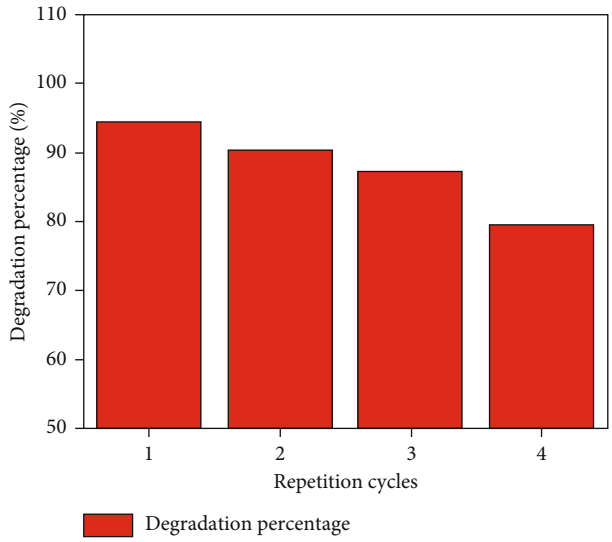

Figure 9: Repetition cycles of MnsR0.75.

$$\mathrm{DE} = 1 - \left(\frac{T}{T_0}\right) \times 100, \tag{2}$$

where DE is the degradation efficiency, T is the concentration of the analyte at time 0 minute, and T_0 is the concentration of the analyte at various time intervals. The photocatalytic performance of the prepared samples was evaluated by the photocatalytic decomposition of aqueous phenol solution under visible light irradiation. From Figure 7, it is evident that rGO exhibits a lower degradation activity than the metal oxide. On further studies at the 120^{th} minute, a total of 33.5% was achieved in the case of pure rGO.

On the other hand, pristine Mn_3O_4 exhibits a degradation of 18.6% at the zeroth minute, and as the time increases with irradiation of visible light, a net degradation of 73.6% was achieved. The composites exhibited an average degradation of 14% at the 0^{th} min, and maximum degradation of 94.48% was achieved for the MnsR0.75 sample (Figures 7(a) and 7(b)).

On further increasing the concentration of Mn_3O_4, it is evident that the degradation percentage decreasing this could be attributed to the agglomeration occurring between the rGO sheets. The $\pi - \pi$ stacking interaction provides a greater amount of phenol concentration near the Mn_3O_4 nanoparticles on the surface of rGO and therefore leads to the more efficient contact between them. Due to its excellent electric conductivity and large specific surface area, it acts as an efficient electron acceptor to enhance the photoinduced charge transfer mechanism. This condition is also hindered in cases when the rGO concentration goes higher as in the MnsR1 composite. Figures 8(a) and 8(b) display the reduction ratio with respect to time. From the degradation percentage, it is evident that the sample MnsR0.75 exhibited the highest degradation, repetition of the experiment was carried out, and the sample was found to degrade around 90%, 87%, and 79% in the repetition cycle as depicted in Figure 9. On further repetition, it was found to decrease to around 52%.

4. Conclusion

In conclusion, Mn_3O_4 nanoparticles were loaded onto the graphene surface by a simple thermal route. Solvent-ethylene glycol played a vital role in the formation of the as-prepared product. The small-sized Mn_3O_4 nanoparticles and high surface area of the reduced graphene oxide composite exhibited better catalytic activity under visible light irradiation. The photocatalyst is highly stable and has been used for four successive times without any significant loss in its activity. The nanocomposite MnsR0.75 exhibited the highest phenol degradation of 94.48%, taking into account the presence of rGO in (i) the utilization of a higher number of photoelectrons and (ii) lowering of electron hole recombination. The high activity exhibited was ascribed due to the strong interaction and progress of synergetic effect between the Mn_3O_4 nanospheres and rGO. Thus, the MnsRnanocomposites can be considered a promising material for the removal of various harmful organic dyes from wastewater.

Data Availability

The data supporting this work is available from the corresponding author upon request.

Conflicts of Interest

The authors declare that they have no conflicts of interest.

References

[1] L. F. Liotta, M. Gruttadauria, G. Di Carlo, G. Perrini, and V. Librando, "Heterogeneous catalytic degradation of phenolic substrates: catalysts activity," *Journal of Hazardous Materials*, vol. 162, no. 2-3, pp. 588–606, 2009.

[2] E. M. Seftel, M. Niarchos, C. Mitropoulos, M. Mertens, E. F. Vansant, and P. Cool, "Photocatalytic removal of phenol and methylene-blue in aqueous media using TiO_2@LDH clay nanocomposites," *Catalysis Today*, vol. 252, pp. 120–127, 2015.

[3] C. Su, X. Duan, J. Miao et al., "Mixed conducting perovskite materials as superior catalysts for fast aqueous-phase advanced oxidation: a mechanistic study," *ACS Catalysis*, vol. 7, no. 1, pp. 388–397, 2017.

[4] L. J. Alemany and M. A. Ban, "Photodegradation of phenol in water using silica-supported titania catalysts," *Applied Catalysis B: Environmental*, vol. 13, no. 3-4, pp. 289–297, 1997.

[5] Y. Liu, L. Yu, C. N. Ong, and J. Xie, "Nitrogen-doped graphene nanosheets as reactive water purification membranes," *Nano Research*, vol. 9, no. 7, pp. 1983–1993, 2016.

[6] R. Kumar, S. Sahoo, E. Joanni et al., "Heteroatom doped graphene engineering for energy storage and conversion," *Materials Today*, vol. 39, pp. 47–65, 2020.

[7] N. Calace, E. Nardi, B. M. Petronio, and M. Pietroletti, "Adsorption of phenols by papermill sludges," *Environmental Pollution*, vol. 118, no. 3, pp. 315–319, 2002.

[8] N. S. Inchaurrondo, P. Massa, R. Fenoglio, J. Font, and P. Haure, "Efficient catalytic wet peroxide oxidation of phenol at moderate temperature using a high-load supported copper catalyst," *Chemical Engineering Journal*, vol. 198-199, pp. 426–434, 2012.

[9] M. Asadollahi-Baboli, "Exploring QSTR analysis of the toxicity of phenols and thiophenols using machine learning methods," *Environmental Toxicology and Pharmacology*, vol. 34, no. 3, pp. 826–831, 2012.

[10] R. Gopal, M. M. Chinnapan, A. K. Bojarajan et al., "Facile synthesis and defect optimization of 2D-layered MoS_2 on TiO_2 heterostructure for industrial effluent, wastewater treatments," *Scientific Reports*, vol. 10, no. 1, p. 21625, 2020.

[11] A. Mohamed, T. A. Osman, M. S. Toprak, M. Muhammed, and A. Uheida, "Surface functionalized composite nanofibers for efficient removal of arsenic from aqueous solutions," *Chemosphere*, vol. 180, pp. 108–116, 2017.

[12] R. Kumar, R. Matsuo, K. Kishida, M. M. Abdel-Galeil, Y. Suda, and A. Matsuda, "Homogeneous reduced graphene oxide supported NiO-MnO_2 ternary hybrids for electrode material with improved capacitive performance," *Electrochimica Acta*, vol. 303, pp. 246–256, 2019.

[13] A. Mohamed, R. El-Sayed, T. A. Osman, M. S. Toprak, M. Muhammed, and A. Uheida, "Composite nanofibers for highly efficient photocatalytic degradation of organic dyes from contaminated water," *Environmental Research*, vol. 145, pp. 18–25, 2016.

[14] F. Zhang, M. Li, W. Li et al., "Degradation of phenol by a combined independent photocatalytic and electrochemical process," *Chemical Engineering Journal*, vol. 175, pp. 349–355, 2011.

[15] D. P. Zagklis, A. I. Vavouraki, M. E. Kornaros, and C. A. Paraskeva, "Purification of olive mill wastewater phenols through membrane filtration and resin adsorption/desorption," *Journal of Hazardous Materials*, vol. 285, pp. 69–76, 2015.

[16] L. D. Naidu, S. Saravanan, M. Goel, S. Periasamy, and P. Stroeve, "A novel technique for detoxification of phenol from wastewater: nanoparticle assisted nano filtration (NANF)," *Iranian Journal of Environmental Health Science & Engineering*, vol. 14, no. 1, p. 9, 2016.

[17] S. Wang, D. Shi, R. Yang, Y. Xu, H. Guo, and X. Yang, "Solvent extraction of phenol from aqueous solution with benzyl 2-ethylhexyl sulfoxide as a novel extractant," *Canadian Journal of Chemical Engineering*, vol. 93, no. 10, pp. 1787–1792, 2015.

[18] N. L. Zabik, C. N. Virca, T. M. McCormick, and S. Martic-Milne, "Selective electrochemical versus chemical oxidation of bulky phenol," *The Journal of Physical Chemistry. B*, vol. 120, no. 34, pp. 8914–8924, 2016.

[19] C. M. Magdalane, K. Kaviyarasu, M. V. Arularasu, K. Kanimozhi, and G. Ramalingam, "Structural and morphological properties of Co_3O_4 nanostructures: investigation of low temperature oxidation for photocatalytic application for waste water treatment," *Surfaces and Interfaces*, vol. 17, p. 100369, 2019.

[20] B. Palanivel, M. Lallimathi, B. Arjunkumar et al., "rGO supported g-C_3N_4/$CoFe_2O_4$ heterojunction: Visible-light-active photocatalyst for effective utilization of H_2O_2 to organic pollutant degradation and $OH^{\bullet}$ radicals production," *Journal of Environmental Chemical Engineering*, vol. 9, no. 1, p. 104698, 2021.

[21] G. Ramalingam, J. Madhavan, P. Sagayaraj, S. Selvakumar, R. Gunaseelan, and R. Jerald Vijay, "Synthesis and characterization of one dimensional semiconducting nanorods and nanobelts," *Transactions of the Indian Institute of Metals*, vol. 64, no. 1-2, pp. 217–220, 2011.

[22] Y. Wang, Y. Xie, H. Sun, J. Xiao, H. Cao, and S. Wang, "2D/2D nano-hybrids of γ-MnO_2 on reduced graphene oxide for catalytic ozonation and coupling peroxymonosulfate activation," *Journal of Hazardous Materials*, vol. 301, pp. 56–64, 2016.

[23] M. Ramesh, M. P. Rao, F. Rossignol, and H. S. Nagaraja, "rGO/MnO2 nanowires for ultrasonic-combined Fenton assisted efficient degradation of reactive black 5," *Water Science and Technology*, vol. 76, no. 7, pp. 1652–1665, 2017.

[24] J. Qu, L. Shi, C. He et al., "Highly efficient synthesis of graphene/MnO_2 hybrids and their application for ultrafast oxidative decomposition of methylene blue," *New York*, vol. 66, pp. 485–492, 2014.

[25] J. Xu, W. Wang, M. Shang, E. Gao, Z. Zhang, and J. Ren, "Electrospun nanofibers of bi-doped TiO_2 with high photocatalytic activity under visible light irradiation," *Journal of Hazardous Materials*, vol. 196, pp. 426–430, 2011.

[26] E. Saputra, S. Muhammad, H. Sun, H.-M. Ang, M. O. Tadé, and S. Wang, "Manganese oxides at different oxidation states for heterogeneous activation of peroxymonosulfate for phenol degradation in aqueous solutions," *Applied Catalysis B: Environmental*, vol. 142-143, pp. 729–735, 2013.

[27] J. C. Contreras-Ruiz, S. Martínez-Gallegos, E. Ordoñez, J. C. González-Juárez, and J. L. García-Rivas, "Synthesis of hydroxide–TiO2 compounds with photocatalytic activity for degradation of phenol," *Journal of Electronic Materials*, vol. 46, no. 3, pp. 1658–1668, 2017.

[28] A. Salama, A. Mohamed, N. M. Aboamera, T. A. Osman, and A. Khattab, "Photocatalytic degradation of organic dyes using composite nanofibers under UV irradiation," *Applied Nanoscience*, vol. 8, no. 1-2, pp. 155–161, 2018.

[29] M. G. Yazdi, M. Ivanic, A. Mohamed, and A. Uheida, "Surface modified composite nanofibers for the removal of indigo carmine dye from polluted water," *RSC Advances*, vol. 8, no. 43, pp. 24588–24598, 2018.

[30] X. Duan, C. Su, L. Zhou et al., "Surface controlled generation of reactive radicals from persulfate by carbocatalysis on nanodiamonds," *Applied Catalysis B: Environmental*, vol. 194, pp. 7–15, 2016.

[31] J. Kang, X. Duan, L. Zhou, H. Sun, M. O. Tadé, and S. Wang, "Carbocatalytic activation of persulfate for removal of antibiotics in water solutions," *Chemical Engineering Journal*, vol. 288, pp. 399–405, 2016.

[32] A. H. Mady, M. L. Baynosa, D. Tuma, and J.-J. Shim, "Facile microwave-assisted green synthesis of Ag- $ZnFe_2O_4$@rGO nanocomposites for efficient removal of organic dyes under UV- and visible-light irradiation," *Applied Catalysis B: Environmental*, vol. 203, pp. 416–427, 2017.

[33] M. M. Kadam, K. B. Dhopte, N. Jha, V. G. Gaikar, and P. R. Nemade, "Synthesis, characterization and application of γ-MnO2/graphene oxide for the selective aerobic oxidation of benzyl alcohols to corresponding carbonyl compounds," *New Journal of Chemistry*, vol. 40, no. 2, pp. 1436–1442, 2016.

[34] T. Zeng, X. Zhang, S. Wang, H. Niu, and Y. Cai, "Spatial confinement of a Co_3O_4 catalyst in hollow metal–organic frameworks as a nanoreactor for improved degradation of organic pollutants," *Environmental Science & Technology*, vol. 49, no. 4, pp. 2350–2357, 2015.

[35] S. Zhang, Q. Fan, H. Gao et al., "Formation of Fe_3O_4@MnO_2 ball-in-ball hollow spheres as a high performance catalyst with enhanced catalytic performances," *Journal of Materials Chemistry A*, vol. 4, no. 4, pp. 1414–1422, 2016.

[36] P. Húmpola, H. Odetti, J. C. Moreno-Piraján, and L. Giraldo, "Activated carbons obtained from agro-industrial waste:

textural analysis and adsorption environmental pollutants," *Adsorption*, vol. 22, no. 1, pp. 23–31, 2016.

[37] J. Zhang, X. Li, H. Chen et al., "Hydrogen production by catalytic methane decomposition: carbon materials as catalysts or catalyst supports," *International Journal of Hydrogen Energy*, vol. 42, no. 31, pp. 19755–19775, 2017.

[38] I. Velo-Gala, J. J. López-Peñalver, M. Sánchez-Polo, and J. Rivera-Utrilla, "Role of activated carbon surface chemistry in its photocatalytic activity and the generation of oxidant radicals under UV or solar radiation," *Applied Catalysis B: Environmental*, vol. 207, pp. 412–423, 2017.

[39] T. Sivakumar Natarajan, H. C. Bajaj, and R. J. Tayade, "Palmyra tuber peel derived activated carbon and anatase TiO_2 nanotube based nanocomposites with enhanced photocatalytic performance in rhodamine 6G dye degradation," *Process Safety and Environment Protection*, vol. 104, pp. 346–357, 2016.

[40] B. Boucher, R. Buhl, and M. Perrin, "Proprietes et structure magnetique de Mn_3O_4," *Journal of Physics and Chemistry of Solids*, vol. 32, no. 10, pp. 2429–2437, 1971.

[41] Y. Cao, X. Lin, C. Zhang et al., "MnO2nanoflakes anchored on reduced graphene oxide nanosheets as high performance anode materials for lithium-ion batteries," *RSC Advances*, vol. 4, no. 57, pp. 30150–30155, 2014.

[42] H. Gao, F. Xiao, C. B. Ching, and H. Duan, "Flexible all-solid-state asymmetric supercapacitors based on free-standing carbon nanotube/graphene and Mn3O4 nanoparticle/graphene paper electrodes," *ACS Applied Materials & Interfaces*, vol. 4, no. 12, pp. 7020–7026, 2012.

[43] H.-L. Guo, X.-F. Wang, Q.-Y. Qian, F.-B. Wang, and X.-H. Xia, "A green approach to the synthesis of graphene nanosheets," *ACS Nano*, vol. 3, no. 9, pp. 2653–2659, 2009.

[44] N. Zhang, C. Fu, D. Liu, Y. Li, H. Zhou, and Y. Kuang, "Three-Dimensional Pompon-like MnO_2/Graphene Hydrogel Composite for Supercapacitor," *Electrochimica Acta*, vol. 210, pp. 804–811, 2016.